Perfluorodecalin Incorporation in Fluorinated Surfactant−Water System: Tailoring of Mesoporous Materials Pore Size

J. L. Blin and M. J. Stébé*

Equipe Physico-chimie des Colloïdes, UMR SRSMC No. 7565, Université Nancy-1/CNRS, Faculté des Sciences, BP 239, F-54506 Vandoeuvre-les-Nancy Cedex, France

Received: February 11, 2004; In Final Form: May 25, 2004

Oil incorporation can strongly affect the phase behavior of surfactant/water systems. In the first part of our experiments, the effect of perfluorodecalin (PFD) addition on the fluorinated surfactant $CF_3(CF_2)_7C_2H_4(OC_2H_4)_9OH$/water system was investigated. L_1 micellar phase, direct hexagonal (H_1), and cubic (I_1) liquid crystals were identified. Phase behavior and SAXS measurements proved that the liquid crystals phase can be swelled by PFD, whereas only 1% of oil can be incorporated into the hydrophobic core of micelles (L_1). Reflections lines of the cubic phase have been indexed in the *Fm*3*m* space group. Large pore mesoporous materials were then synthesized by incorporating PFD as a swelling agent. The present work shows that PFD is an effective expander to enlarge the pore size of mesoporous materials. Characterization of the recovered materials and evolution of $CF_3(CF_2)_7C_2H_4(OC_2H_4)_9OH$/water system with PFD loading led us to propose a mechanism describing the swelling effect of PFD.

1. Introduction

$C_m{}^F(EO)_n$ surfactants are the fluorinated analogues of the hydrogenated polyoxyethylene alkyl ethers [$C_m(EO)_n$]. Hydrogenated surfactants are used in various domains as emulsifiers, wetting agents, detergents, or solubilizers. The introduction of fluorine atoms strongly affects the properties of the surfactant,[1] and peculiar applications can be considered. Indeed, linear fluorocarbon chains are less flexible than the hydrocarbon ones and, thus, present high melting points. Moreover, the capacity of fluorocarbons to dissolve high quantities of oxygen and carbon dioxide makes them very attractive for biomedical applications such as oxygen vectorization.[2,3] Nevertheless, both families adopt similar behavior in solution,[4,5] and those surfactants can be employed for the preparation of mesoporous materials. Using polyoxyethylene alkyl ethers, a series of compounds labeled for example SBA[6,7] (Santa Barbara) and MSU[8,9] (Michigan State University) have been prepared. Recently, we reported the synthesis of mesoporous materials using a nonionic fluorinated surfactant.[10] As regards the synthesis of mesoporous molecular sieves, the main advantage of fluorinated surfactants compared to the hydrogenated ones is their high thermal stability. Indeed, with silica-based materials, a critical factor in increasing the hydrothermal stability is to get more silica condensation on the pore walls.[11−13] With hydrogenated surfactants, the preparation is performed at low temperature, and these synthesis conditions lead to imperfectly condensed mesoporous walls with large amounts of terminal hydroxyl groups that make the mesostructure unstable, especially under hydrothermal or steam conditions.[14] Replacing the hydrogenated surfactant by a fluorinated one, as the hydrothermal treatment can be performed at higher temperature, we could expect that the level of silica condensation would be enhanced and, thus, that the recovered materials would exhibit a higher hydrothermal stability. These silica supports are of particular interest in the preparation of catalysts,[15−17] drug delivery systems,[18] and sensors.[19] However, before developing such applications, it is also important to tailor the pore size diameter. For example, some technologically important catalytic treatments of organic molecules such as the ammoxidation of hydroxyacetophenones,[15] the selective oxidation of aromatics,[20] the hydroxylation of phenols,[16] and vinyl acetate production[17] require supports that exhibit quite large pore diameters in addition to high surface area and stability. Postsynthesis treatments,[21,22] surfactants of different chain length,[23] or swelling agent incorportation can lead to the preparation of large pore mesoporous materials. In the literature, 1,3,5-trimethylbenzene (TMB),[24−26] triisopropylbenzene,[27] amines,[28] and alkane[29−31] have been used as expanders. However, the introduction of organic auxiliaries will strongly affect the surfactant behavior in solution and, thus, the mesoporous structure. Since fluorinated surfactants allow cosolubilization of water and perfluoroalkanes,[32,33] perfluorodecalin (PFD) has been employed as swelling agent in the present study in order to obtain large pore silica mesoporous materials using a nonionic fluorinated surfactant $CF_3(CF_2)_7C_2H_4(OC_2H_4)_9OH$. We have investigated the effect of this fluorocarbon addition on the surfactant phase behavior in water and tried to provide possible explanation concerning the swelling mechanism of mesoporous materials.

2. Materials and Methods

2.1. Sample Preparation. *Phase Diagram Determination.* The used fluorinated surfactant, which was provided by DuPont, had an average chemical structure of $CF_3(CF_2)_7C_2H_4(OC_2H_4)_9OH$, labeled as $R^F{}_8(EO)_9$ (or FSN-100, its commercial name). The surfactant hydrophilic chain moiety exhibited a Gaussian chain length distribution. The samples were prepared by weighing the required amounts of surfactant, oil, and water in well-closed glass vials to avoid evaporation. They were left at controlled temperature for some hours in order to reach equilibrium. The phase diagram was established between 10 and 60 °C in the whole water−surfactant composition. Oil

* Corresponding author: Ph +33-3-83-68-43-43; Fax +33-3-83-68-43-22; e-mail Marie-Jose.Stebe@lesoc.uhp-nancy.fr.

10.1021/jp049379s CCC: $27.50
Published on Web 07/01/2004

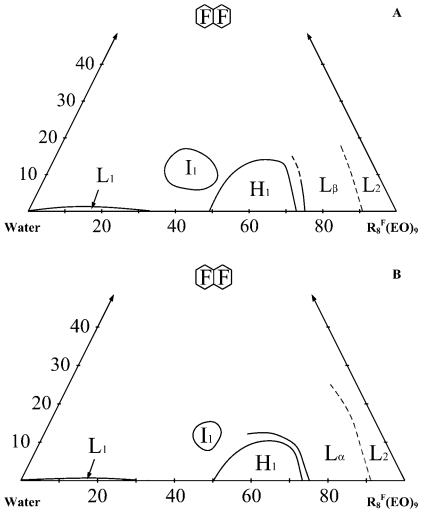

Figure 1. Temperature−composition phase diagram (wt %) of $R^F_8(EO)_9/C_{10}F_{18}$/water system at 20 °C (A) and 50 °C (B).

concentration was made to vary from 1 to 30 wt %. Liquid crystal phase domains were identified by their texture observed with optical microscope equipped with cross polarizers. To find the exact limits of these domains, additional SAXS measurements were also performed at LURE (Orsay, France) on beamline D22 of the DCI synchrotron. The incident beam wavelength λ was 1.39 Å, and the sample-to-detector distance was 1800 mm.

Mesoporous Preparation. Before the incorporation of perfluorodecalin (PFD), a micellar solution of $R^F_8(EO)_9$ containing 10 wt % in water was prepared. The concentration of PFD ($C_{10}F_{18}$), added to the micellar solution, was made to vary from 1 to 40 wt %, which corresponds to a variation of the $C_{10}F_{18}/R^F_8(EO)_9$ molar ratio from 0.018 to 1.255. The pH value of the solution was then adjusted to 2.0 using sulfuric acid. Tetramethoxysilane (TMOS), used as the silica source, was added dropwise. The surfactant/silica molar ratio was adjusted to 0.5. The obtained gel was sealed in Teflon autoclaves and heated for 1 day at 80°C. The final products were recovered after ethanol extraction with a Soxhlet apparatus during 30 h.

Mesoporous Characterization. X-ray measurements were carried out using a home-built apparatus, equipped with a classical tube (λ = 1.54 Å). The X-ray beam was focused by means of a curved gold/silica mirror on the detector placed at 527 nm from the sample holder. Nitrogen adsorption−desorption isotherms were obtained at −196 °C over a wide relative pressure range from 0.01 to 0.995 with a volumetric adsorption analyzer TRISTAR 3000 manufactured by Micromeritics. The samples were degassed further under vacuum for several hours at 320 °C before nitrogen adsorption measurements. The pore diameter and the pore size distribution were determined by the BJH (Barret, Joyner, Halenda) method.[34]

3. Results and Discussion

3.1. $R^F_8(EO)_9/C_{10}F_{18}$/Water System. A partial phase diagram of the ternary $R^F_8(EO)_9/C_{10}F_{18}$/water system is reported in Figure 1 at 20 °C (Figure 1A) and 50 °C (Figure 1B). In the investigated temperature range, the liquid crystal domain is composed of the cubic, hexagonal, and lamellar phases. The last two ones are already present in the binary system.[10]

At high water concentration, the existence range of the micellar domain (L_1) is small; only 1 wt % of $C_{10}F_{18}$ can be incorporated in micelles. If the PFD loading is increased, a Winsor I solution is obtained. The upper phase is composed of the swollen micelles, whereas the PFD excess constitutes the lower phase. Between 35 and 50 wt % of $R^F_8(EO)_9$, a cubic phase, which is not observed in the binary system, is formed between 8 and 17 wt % of oil. The existence range of the cubic structure is limited. When the weight percent of surfactant is increased from 50 to 72 wt %, an optically anisotropic phase is detected. The fan-shaped texture observed by optical microscopy with polarized light is characteristic of the defects of the direct hexagonal H_1 phase. The hexagonal symmetry is confirmed by SAXS measurements. Indeed, lines located at 6.82 and 3.97 nm, for the sample prepared with 54.5 wt % of $R^F_8(EO)_9$, 9.1 wt % of PFD, and 36.4 wt % of water, are detected on the pattern (Figure 2). The relative positions of the Bragg reflections are 1, $\sqrt{3}$. Consequently, they can be attributed to the (100) and (110) reflections of the hexagonal structure. Contrary to the hydrogenated system, the (200) reflection is not observed for this fluorinated surfactant. The surfactant range composition belonging to H_1 is progressively reduced as the PFD loading is increased. Indeed, as it can be seen in Figure 1, the $C_{10}F_{18}$ incorporation rate in the hexagonal phase is strongly dependent on the $R^F_8(EO)_9$/water ratio (noted R), and it reaches a maximum (14.0 wt %) for R = 2.28. The H_1 phase is separated from the cubic one by a two-phase region. If the surfactant concentration is further increased (>73 wt %), the lamellar (L_α) or the gel phase (L_β) appears. The liquid crystal domain is progressively reduced as the temperature increases from 20 to 60 °C, and only the lamellar phase remains above 60 °C.

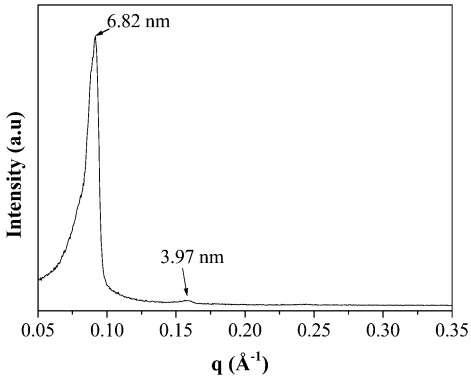

Figure 2. Hexagonal SAXS pattern at 25 °C of sample prepared with 54.5 wt % of $R^F_8(EO)_9$, 9.1 wt % of $C_{10}F_{18}$, and 36.4 wt % of water.

a. Hexagonal Phase (H_1). The hexagonal phase is composed of infinite cylinders packed in a hexagonal array. In the case of direct systems, cylinders are filled first by the hydrophobic chains, eventually by oil, and are covered by both headgroups and water. The hexagonal H_1 phase is characterized by its typical SAXS profile with the relative peak positions, 1, $\sqrt{3}$, 2. The distance d associated with the first peak is related to the hydrophobic radius R_H by the relation[35]

$$\frac{V_B + \beta V_O}{V_S + \alpha V_W + \beta V_O} = \frac{\sqrt{3}\pi R_H^2}{2d^2}$$

where α and β respectively stand for the number of water and oil molecules per surfactant molecule, and V_B, V_S, V_W, and V_O respectively stand for the molar volumes of the hydrophobic part of the surfactant (V_B = 261 cm^3/mol), the surfactant (V_S = 626 cm^3/mol), water (V_W = 18 cm^3/mol), and oil (V_O = 237 cm^3/mol). The cell parameter a is given by the relation $a = 2d/\sqrt{3}$. Results concerning different $R^F_8(EO)_9$/water ratios (R) are reported in Figure 3A,B. For a given R, as shown in Figure 3A, an increase in the d spacing and, thus, in the cell parameter

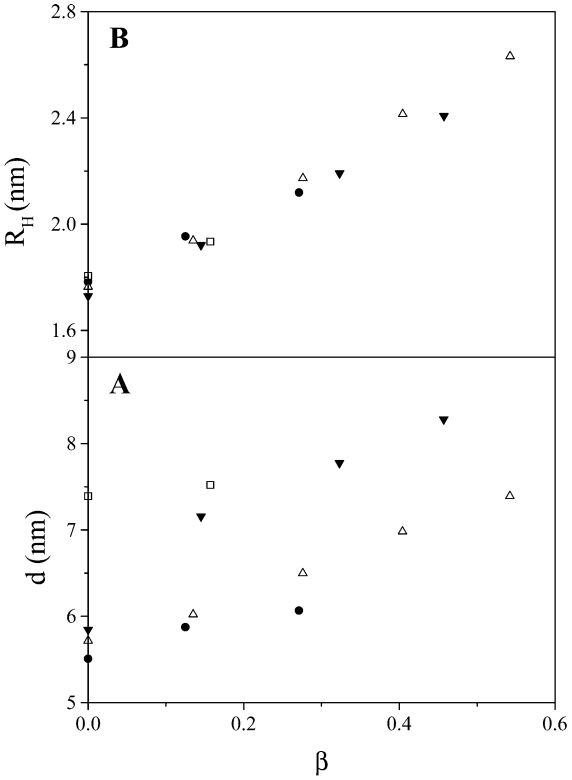

Figure 3. Hexagonal liquid crystal $R^F_8(EO)_9/C_{10}F_{18}$/water: (A) repetition distance (d) and (B) hydrophobic radius (R_H) as a function of β the number of oil molecules per surfactant molecule for different $R^F_8(EO)_9$/water ratios (R) [●, $R = 3$; △, $R = 2.28$; ▼, $R = 1.85$; □, $R = 1.5$].

TABLE 1: Hexagonal Liquid Crystal[a]

β	d (nm)	a (nm)	R_H (nm)	S (nm^2)
0	5.7	6.6	1.8	0.49
0.135	6.0	6.9	1.9	0.48
0.276	6.5	7.5	2.2	0.50
0.404	7.0	8.1	2.4	0.49
0.542	7.4	8.5	2.6	0.49

[a] Repetition distance (d), cell parameter (a), hydrophobic radius (R_H), and cross-sectional area (S) as a function of β, the number of oil molecules per surfactant molecule. The $R^F_8(EO)_9$/water ratio is fixed to 2.28.

is noted with increasing oil content. Incorporation of $C_{10}F_{18}$ also leads to an increase in R_H (Figure 3B). For example, R_H varies from 1.8 to 2.6 nm when β is changed from 0 to 0.542 ($R = 2.28$).

The cross-sectional area S can then be deduced from the following relation:

$$S = \frac{2(V_B + \beta V_O)}{0.6R_H}$$

The cross-sectional area remains constant in the overall H_1 domain, and as indicated Table 1, its value is 0.49 ± 0.01 nm^2. According to previous work,[36,37] when oil such as $C_{10}F_{18}$ is added, it either penetrates into the amphiphilic film (penetration effect) or forms a core (swelling effect). Both effects can also simultaneously occur. In a paper dealing with the effect of oil on the structure of liquid crystals in polyoxyethylene dodecyl ether−water systems, Kunieda et al.[38] reported that saturated hydrocarbons such as decane favor a swelling of the hexagonal structure core cylinders, whereas aromatic hydrocarbons such as *m*-xylene tend to penetrate the surfactant palisade layer.

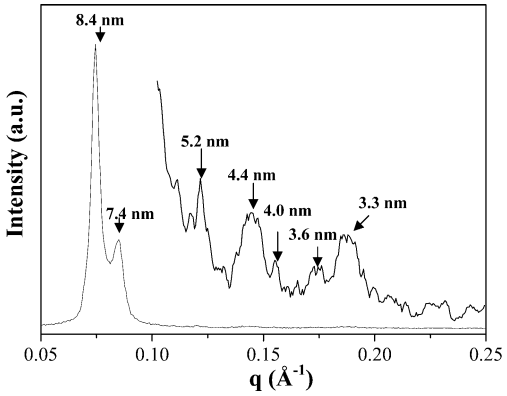

Figure 4. Typical SAXS pattern of cubic liquid crystal.

Concerning the $R^F_8(EO)_9$/water system, we recently[10] showed that the hydrophobic chains in the H_1 liquid crystal phase are completely extended. Indeed, the size of the hydrophobic core cylinders corresponds to the length of an alkyl chain with 10 carbon atoms adopting a zigzag conformation. In the ternary $R^F_8(EO)_9/C_{10}F_{18}$/water system, since the cross-sectional area value remains unchanged compared to the binary system, we can assume that the hydrophobic chains in the H_1 liquid crystal phase also adopt a zigzag conformation. The increase in the R_H value with oil loading, for a given $R^F_8(EO)_9$/water ratio, indicates that PFD is truly entrapped into the hydrophobic core of the rods. From this observation it is obvious that PFD is incorporated into the core of micelles, whereas penetration of PFD between the hydrophobic chains is not favored as observed for decane in the hydrogenated system.

b. Cubic Phase (I_1). There are two classes of cubic phases. The first one consists of bicontinuous cubics, denoted V, and their basic structure is fine. The segregation of the aqueous and nonaqueous domains is obtained by the constitution of two overlapped but not connected networks, and two space groups *Pn*3*m*[39] and *Ia*3*d*[40] have been unambiguously identified. This kind of cubic structure is usually observed in $C_m(EO)_n$/water, $C_m{}^F(EO)_n$/water, and lipid/water systems. The second family deals with the micellar cubics (I), which consist of discrete micellar aggregates arranged on cubic lattices. Two space groups *Pm*3*n* and *Fd*3*m* have been identified. The first one is associated with a direct structure, whereas the second one is encountered for the reverse cubic phase. As concerns the direct structure, two novel space groups *Im*3*m* and *Fm*3*m* have recently been evidenced.[41,42] The position of the cubic domain in the phase diagram represented in Figure 1 strongly suggests that the cubic structure evidenced in the $R^F_8(EO)_9/C_{10}F_{18}$/water system should belong to the family of direct micellar cubic structures. Since the SAXS pattern is rather poor, space group identification of this type of cubic phase is not easy. Indeed, different authors[41,43] tried to provide further information about the nature of the cubic structure, and the debate is still open. Nevertheless, in a study dealing with the micellar cubic phase encountered in the nonionic surfactant $C_{12}(EO)_{12}$/water system, Tiddy et al.[42] have clearly identified three cubic phases by small-angle X-ray diffraction. The powder diffraction indexation has evidenced that these cubic phases belong to the *Im*3*m*, *Pm*3*m*, and *Fm*3*m* space groups. Because of their position in the phase diagram, at higher hydratation compared to that of the H_1 phase, the authors concluded that all three cubic structures were I_1 phases.

A typical scattering spectrum of samples belonging to the cubic domain, in the $R^F_8(EO)_9/C_{10}F_{18}$/water system, is reported in Figure 4. The relative positions of the Bragg reflections are $\sqrt{(4/3)}$, $\sqrt{(8/3)}$, $\sqrt{(11/3)}$, $\sqrt{(12/3)}$, $\sqrt{(16/3)}$, and $\sqrt{(20/3)}$.

TABLE 2: Cubic Liquid Crystal[a]

hkl	$h^2 + k^2 + l^2$	d_{obs} (nm)	I_{obs}
111	3	8.4	vs
200	4	7.4	s
220	8	5.2	m
311	11	4.4	m
222	12	4.0	w
400	16	3.6	w
420	20	3.3	m

[a] X-ray diffraction data of sample $R^F_8(EO)_9/C_{10}F_{18}$/water; $R = 0.968$ and $\beta = 0.38$. Indexed in the space group $Fm3m$ with a lattice parameter $a = 14.5$ nm.

TABLE 3: Cubic Liquid Crystal[a]

R	β	d (nm)	a (nm)	R_H (nm)	S (nm^2)
0.670	0.46	9.28	16.08	3.56	0.52
0.766	0.46	9.10	15.76	3.59	0.52
0.968	0.38	8.38	14.51	3.43	0.51
	0.57	9.16	15.86	3.86	0.51

[a] Repetition distance (d), cell parameter (a), hydrophobic radius (R_H), and cross-sectional area (S) as a function of β, the number of oil molecules per surfactant molecule.

According to results published by Tiddy et al.,[42] they can be indexed in the $Fm3m$ space group (Table 2), and their relative intensities, given in Table 2, are in good agreement with those reported by these authors.[42] This micellar cubic phase consists of discrete micellar aggregates embedded in a continuous water matrix and can be described as a packing of quasi-spherical micelles on a face-centered-cubic lattice. To pack space completely, each micelle, along with surrounding water, will present the average shape of a dodecahedron. These dodecahedra subsequently pack together to form the complete structure. In this case, the relation between the cell parameter ($a = d_{111}\sqrt{3}$) and the hydrophobic radius R_H becomes

$$\frac{V_B + \beta V_O}{V_S + \alpha V_W + \beta V_O} = \frac{16\pi {R_H}^3}{3a^3}$$

The cross-sectional area S can then be deduced from the following relation:

$$S = \frac{3(V_B + \beta V_O)}{0.6R_H}$$

From Table 3, which depicts results obtained for the cubic liquid crystal, it appears that the cross-sectional area remains constant at about 0.51 ± 0.01 nm^2. As values of cross-sectional area in the hexagonal H_1 (0.49 nm^2) and cubic I_1 (0.51 nm^2) phase are closed, it can be assumed that the hydrophobic chains in the cubic structure also adopt a zigzag conformation. The increase in R_H with oil incorporation reveals that the swelling effect occurs and that PFD is truly entrapped in the hydrophobic core of the micelles (I_1). For example, in the case of a $R^F_8(EO)_9$/water ratio of 0.968, R_H varies from 3.43 to 3.86 nm, when the number of oil molecules per surfactant molecule changes from 0.38 to 0.57 (Table 3).

3.2. Large Pore Mesoporous Materials. After investigating the phase diagram and evaluating the liquid crystal structural parameters of the ternary $R^F_8(EO)_9/C_{10}F_{18}$/water system, we used PFD as organic auxiliary to prepare mesoporous materials. Synthesis conditions such as weight percent of $R^F_8(EO)_9$ in water, $R^F_8(EO)_9$/silica molar ratio, heating temperature, and duration have been adjusted according to a previous study.[10]

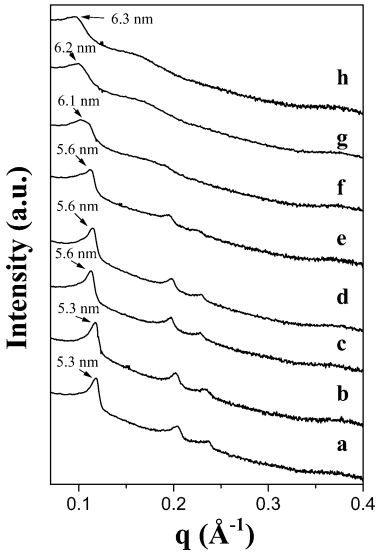

Figure 5. Mesoporous materials: SAXS patterns of samples synthesized with a $C_{10}F_{18}/R^F_8(EO)_9$ molar ratio of (a) 0, (b) 0.067, (c) 0.113, (d) 0.209, (e) 0.399, (f) 0.471, (g) 0.628, and (h) 1.255.

TABLE 4: Mesoporous Materials[a]

$C_{10}H_{18}/R^F_8(EO)_9$ molar ratio	structure	a_0 (nm)	pore diameter (nm)[b]	wall thickness (nm)
0	hexagonal	6.1	4.6	1.5
0.018	hexagonal	6.1	5.0	1.1
0.067	hexagonal	6.1	5.0	1.1
0.113	hexagonal	6.5	5.0	1.5
0.209	hexagonal	6.5	5.4	1.1
0.399	hexagonal	6.5	5.8	0.7
0.471	wormhole		6.0	
0.628	wormhole		6.3	
0.807	wormhole		6.4	
1.255	wormhole		6.7	

[a] Structure, values of cell parameter (a_0), pore diameter, and wall thickness as a function of the $C_{10}H_{18}/R^F_8(EO)_9$ molar ratio. [b] Values obtained from BJH method applied to the adsorption branch of the isotherm.

As regards materials obtained with a $C_{10}F_{18}/R^F_8(EO)_9$ molar ratio comprised between 0 and 0.399, in addition to a sharp peak at 5.6 nm, two other peaks are detected on the SAXS pattern (Figure 5a−e). The presence of these last two peaks is characteristic of a hexagonal organization of the channels. Indeed, it was reported[44] that X-ray diffractograms of powdery hexagonal mesoporous materials exhibit a typical three-peak pattern with a very strong feature at a low angle (100 reflection line) and two other weaker peaks at higher angles (110 and 200 reflection lines). The unit cell a_0, which is the sum of the pore diameter and of the thickness of the pore wall, can be deduced from the following relation: $a_0 = 2d_{100}/(3)^{1/2}$, and its value varies from 6.1 to 6.5 nm with the increase in PFD loading (Table 4). The wall thickness is deduced by subtracting the pore size determined by the BJH method (see below) from the dimension of the unit cell. The slight increase in a_0 value associated with the decrease in wall thickness, observed when the PFD/surfactant molar ratio is raised, indicates the enlargement effect of PFD on the pore size.

If PFD is further added into the micellar solution ($C_{10}F_{18}/R^F_8(EO)_9$ molar ratio > 0.399), no secondary reflections are detected any longer (Figure 5f−h). Thus, the regular channel array is lost, and the presence of a single reflection indicates the formation of a disordered structure. In this case, the recovered mesoporous molecular sieves exhibit a wormhole-like channel system, analogous to MSU-type materials. The

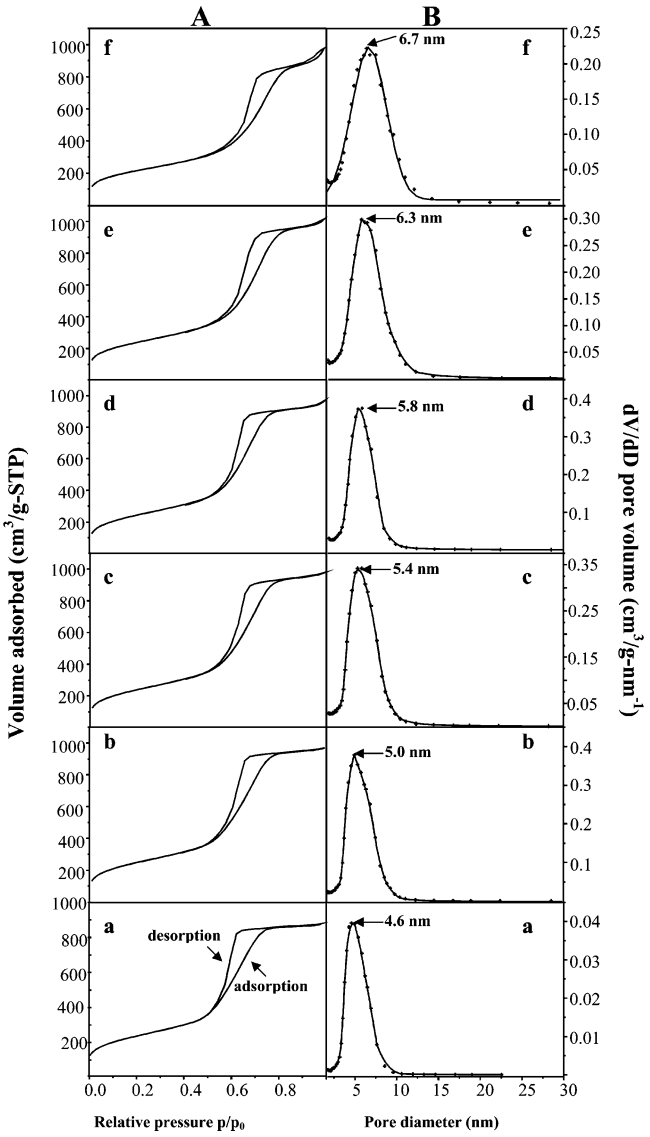

Figure 6. Nitrogen adsorption−desorption isotherms (A) and pore size distribution (B) of samples synthesized with a $C_{10}F_{18}/R^F_8(EO)_9$ molar ratio of (a) 0, (b) 0.067, (c) 0.209, (d) 0.399, (e) 0.628, and (f) 1.255.

broad peak that is observed on the XRD pattern is an indication of the average pore-to-pore separation in the disordered wormhole framework, which presents a lack of long-range crystallographic order. In this case, the addition of PFD disfavors the formation of the hexagonal structure.

Figure 6 depicts the nitrogen adsorption−desorption isotherms (Figure 6A) and the pore size distribution (Figure 6B) of the material obtained with different $C_{10}F_{18}/R^F_8(EO)_9$ molar ratios. A IV-type nitrogen isotherm (Figure 6A), characteristic of mesoporous compounds according to the BDDT classification,[45] is obtained. With increasing the PFD/surfactant molar ratio, the relative pressure for which capillary condensation takes place is shifted toward higher values. Since the p/p_0 position of the inflection point is related to the pore diameter, it can be inferred that an enlargement of the mean pore diameter occurs when the loading of oil is raised. This increase in pore diameter is further confirmed by the pore size distribution (Figure 6B), whose maximum is shifted from 4.6 to 6.7 nm when the $C_{10}F_{18}/R^F_8(EO)_9$ molar ratio is progressively increased from 0 to 1.255 (Figure 6B). Moreover, for materials prepared with low $C_{10}F_{18}/R^F_8(EO)_9$ molar ratio, the pore size distribution is rather narrow

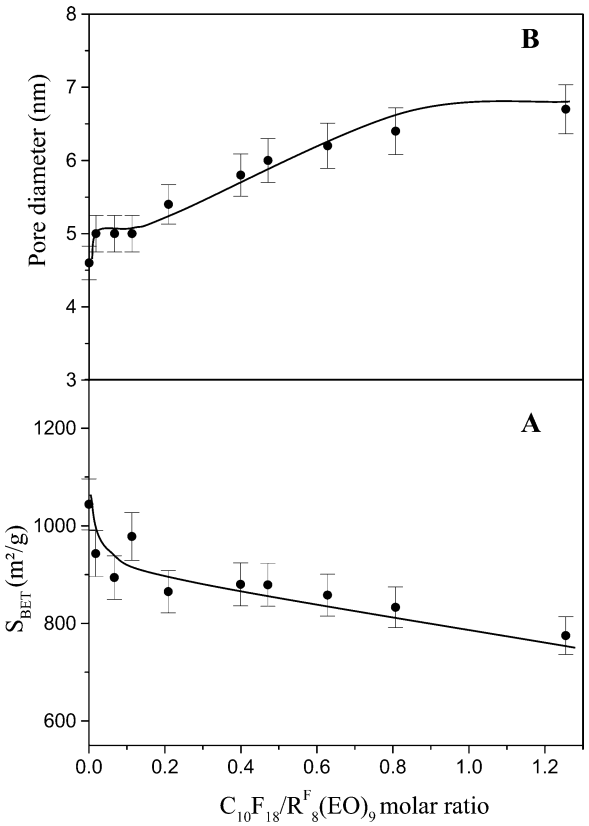

Figure 7. Variation of the specific surface area (A) and the pore diameter (B) with the $C_{10}F_{18}/R^F_8(EO)_9$ molar ratio.

(Figure 6Ba−d) and becomes broader with further PFD incorporation (Figure 6B).

The shape of the hysteresis loop is slightly modified with increasing the PFD loading. Low $C_{10}F_{18}/ R^F_8(EO)_9$ molar ratios rather lead to H_1 whereas a H_2 type is observed for higher ratios. This change can be related to the transition from a well-ordered to a disordered channel array. Indeed, H_2 is often encountered for disordered materials with a wormhole structure.

Whatever the $C_{10}F_{18}/R^F_8(EO)_9$ molar ratio, the specific surface area is rather high (>700 m^2/g). However, its values slowly decreases with the incorporation of PFD (Figure 7A), reflecting the progressive disorganization of the channel array.

3.3. Discussion. Several groups attempt to expand the pore size of mesoporous materials, but only few of them have tried to suggest a detailed swelling mechanism. For example, Ulagappan et al.,[29] dealing with alkane incorporation and micellar system organization using a cationic surfactant in the process of mesoporous silica formation, indicated, on the basis of XRD and nitrogen adsorption results, that, for short alkanes, the solubilizing agent penetrates between the tails of surfactant molecules. On the contrary, for higher alkanes, such as decane, the alkane molecules form a core which is then surrounded by a layer of the cationic surfactant molecules, and the swelling mechanism involves one molecule of surfactant for one molecule of expander. Using nonionic polyoxyethylene surfactant, Boissière et al.[46] consider a swelling effect of the micelle core to explain the effect of the addition of a swelling agent (TMB) on the pore size of MSU mesoporous silica. However, no study was performed to understand the effect of TMB addition on micelles in water.

The results obtained in the present study lead us to conclude that such a mechanism is not applicable for the mesoporous prepared from $R^F_8(EO)_9$ and $C_{10}F_{18}$ as organic auxiliary. Indeed, in the first part of this paper, we have evidenced that only a

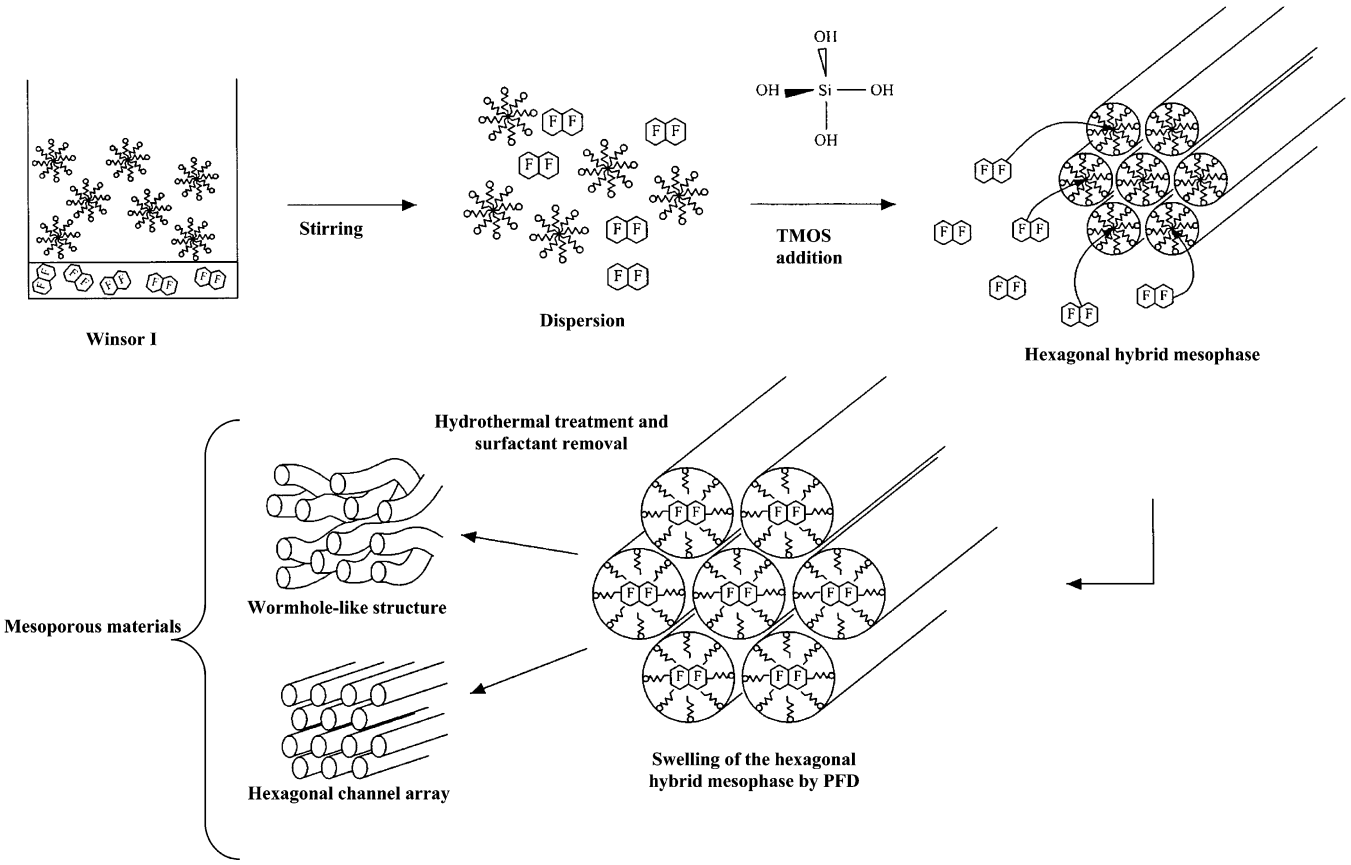

Figure 8. Scheme of the proposed swelling mechanism of mesoporous materials pore size.

very small quantity (≈1 wt %) of PFD can be incorporated into the micelles (L_1) of $R^F_8(EO)_9$ in water. Increasing the amount of PFD leads to a biphasic system (Winsor I), as the excess of PFD is in equilibrium with the swollen micelles in water. Thus, in this case, the pore size enlargement cannot be due to a swelling effect of the hydrophobic micelle core. Nevertheless, we have shown that PFD can be incorporated into the H_1 liquid crystal and that it swells the core cylinders of the hexagonal structure. On the basis of results obtained from the investigation of the phase diagram of the ternary $R^F_8(EO)_9/C_{10}F_{18}$/water system, we suggested the mechanism represented in Figure 8 to explain the pore size expansion of mesoporous molecular sieves.

First, the addition of $C_{10}F_{18}$ (>1 wt %) into the micellar solution of $R^F_8(EO)_9$ in water involves the formation of a Winsor I system. As represented in Figure 8, a very weak fraction of oil is incorporated in the hydrophobic micelle core (1 wt %), and a separation occurs between these slightly swollen micelles and excess PFD. The quantity of PFD incorporated into the micelle is not sufficient to explain the mesoporous pore size expansion. When TMOS is added to the surfactant, water, and oil mixture, hydrogen-bonding interactions between the oxygen atoms of the oxyethylene group of the surfactant and hydrogen atoms of TMOS are formed. To complete polymerization of tetramethoxysilane, these supramolecular assemblies (surfactant−silica) have to pack together, leading to the formation, through a CTM (cooperative templating mechanism)-type mechanism,[7,47,48] of a hexagonal hybrid mesophase, whose features are analogous to the H_1 liquid crystal.[10] Then, because of stirring, PFD can be incorporated in this hybrid hexagonal mesophase, involving a channel swelling. The hydrothermal treatment at 80 °C completes the polymerization of the silica source, and after surfactant removal by ethanol extraction, large pore mesoporous materials with pore size up to 5.8 nm are obtained. It should be reminded that the CTM mechanism is described as follows: in the initial step, the interactions between silica and isolated spherical or cylindrical micelles drive to the formation of an organic−inorganic mesophase. Then, the condensation of the inorganic precursor at the external surface of the micelles occurs. The ordered mesophase is obtained after intermicellar condensation. Finally, the hydrothermal treatment at higher temperature completes the assembly and the polymerization of the silica source.

However, if the $C_{10}F_{18}/R^F_8(EO)_9$ molar ratio is superior to 0.399, the expansion of the pore size still occurs, and the value of the pore diameter can reach 6.7 nm, but the recovered materials adopt a wormhole-like structure. This observation is in good agreement with the evolution of the phase diagram reported above. Indeed, we have evidenced that the surfactant range composition belonging to H_1 is progressively reduced with $C_{10}F_{18}$ incorporation. Thus, it can be assumed that the hexagonal hybrid mesophase is disorganized if the $C_{10}F_{18}$ content is too high, as observed for the H_1 liquid crystal, which can incorporate up to 14.00 wt % of PFD at 20 °C.

4. Conclusions

The phase diagram of the ternary $R^F_8(EO)_9/C_{10}F_{18}$/water system was first investigated. We have delimited the different phase domains and determined the structural parameters of the H_1 and I_1 liquid crystals. To our knowledge, it is the first time that the space group *Fm*3*m* has been evidenced for a system with a fluorinated surfactant. We have shown that the hydrophobic chains are completely extended and that PFD can swell H_1 and I_1 structures, whereas only 1 wt % of $C_{10}F_{18}$ can be incorporated in micelles (L_1) of fluorinated surfactant in water.

Increasing the PFD content involves the formation of a Winsor I system. The composition range of the cubic structure is limited.

The present study also reveals that PFD can be used as a swelling agent to enlarge the pore size of mesoporous materials. The pore diameter of the channels can be expanded from 4.6 to 6.7 nm by varying the $C_{10}F_{18}/R^F{}_8(EO)_9$ molar from 0 to 1.255. Fine hexagonal mesoporous materials are synthesized at low $C_{10}F_{18}/R^F{}_8(EO)_9$ molar ratio (until 0.399), whereas a wormhole-like structure is formed with higher PFD loading.

On the basis of the $R^F{}_8(EO)_9/C_{10}F_{18}$/water system, we suggested a mechanism to account for the enlargement of the pore size of mesoporous materials by PFD. We have shown that the swelling of a hexagonal hybrid mesophase (surfactant-silica) can be related to PFD incorporation in hexagonal liquid crystal H_1.

Acknowledgment. The authors thank C. Brioual and A. Grandmougin for their contribution to this work as well as DuPont de Nemours Belgium for providing the $R^F{}_8(EO)_9$ (FSN-100) and P. Lesieur and C. Borde for their assistance during SAXS experiments. The authors also thank A. Fischer for revising the English.

References and Notes

(1) Shinoda, K.; Hato, M.; Hayashi, T. *J. Phys. Chem.* **1988**, *76*, 234.
(2) Riess, J. G. *Chem. Rev.* **2001**, *101*, 2797.
(3) Krafft, M. P. *Adv. Drug Delivery Rev.* **2001**, *47*, 209.
(4) Ravey, J. C.; Stébé, M. J. *Prog. Colloid Polym. Sci.* **1988**, *76*, 234.
(5) Ravey, J. C.; Stébé, M. J. *Colloids Surf. A: Physicochem. Eng. Aspects* **1994**, *84*, 11.
(6) Huo, Q.; Margolez, D. I.; Stucky, G. D. *Chem. Mater.* **1996**, 8 1147.
(7) Zhao, D.; Huo, Q.; Feng, J.; Chmelka, B. F.; Stucky, G. D. *J. Am. Chem. Soc.* **1998**, *120*, 6024.
(8) Bagshaw, S. A.; Prouzet, E.; Pinnavaia, T. J. *Science* **1995**, *269*, 1242.
(9) Prouzet, E.; Pinnavaia, T. J. *Angew. Chem., Int. Ed. Engl.* **1997**, *36*, 516.
(10) Blin, J. L.; Lesieur, P.; Stébé, M. J. *Langmuir* **2004**, *20*, 491.
(11) Kim, S. S.; Zhang, W.; Pinnavaia, T. J. *Science* **1998**, *282*, 1032.
(12) Mokaya, R. *Angew. Chem., Int. Ed.* **1999**, *38*, 2930.
(13) Mokaya, R. *J. Phys. Chem. B* **1999**, *103*, 10204.
(14) Corma, A. *Chem. Rev.* **1997**, *97*, 2373.
(15) Clerici, M. G. *Appl. Catal.* **1991**, *68*, 249.
(16) Clerici, M. G.; Ingallina, P. *J. Catal.* **1993**, *140*, 71.
(17) Nakamura, S.; Yasui, T. *J. Catal.* **1970**, *17*, 336.
(18) Vallet-Regi, M.; Ramila, A.; Del Real, R. P.; Pérez-Pariente, J. *Chem. Mater.* **2001**, *13*, 308.
(19) Walcarius, A.; Lüthi, N.; Blin, J. L.; Su, B. L.; Lamberts, L. *Electrochim. Acta* **1999**, *44*, 4601.
(20) Tanev, P. T.; Pinnavaia, T. J. *Science* **1995**, *267*, 865.
(21) Huo, Q.; Margolese, D. I.; Stucky, G. D. *Chem. Mater.* **1996**, *8*, 1147.
(22) Sayari, A.; Liu, P.; Kruk, M.; Jaroniec, M. *Chem. Mater.* **1997**, *9*, 2499.
(23) Sayari, A.; Karra, V. R.; Sudhakar Reddy, J. Symposium on Synthesis of Zeolites, Layered Compounds and Other Microporous Solids, 209th National Meeting of the American Chemical Society, Anaheim, 1995.
(24) Beck, J. S. U.S. Patent 5, 057296, 1991.
(25) Branton, J.; Dougherty, J.; Lockhart, G.; White, J. W. *Charact. Porous Solids IV* **1997**, 668.
(26) Desplantier-Giscard, D.; Galarneau, A.; Di Renzo, F.; Fajula, F. *15 Âme réunion du Groupe Français des Zéolithes*, Carry Le Rouet, 1999.
(27) Kimura, T.; Sugahara, Y.; Kuroda, K. *Chem. Commun.* **1998**, 559.
(28) Sayari, A.; Kruk, M.; Jaroniec, M.; Moudrakovski, I. L. *Adv. Mater.* **1998**, *10*, 1376.
(29) Ulagappan, N.; Rao, C. N. R. *Chem. Commun.* **1996**, 2759.
(30) Blin, J. L.; Otjacques, C.; Herrier, G.; Su, B.-L. *Langmuir* **2000**, *16*, 4229.
(31) Blin, J. L.; Su, B.-L. *Langmuir* **2002**, *18*, 5303.
(32) Mathis, G.; Leempoel, P.; Ravey, J. C.; Selve, C.; Delpuech, J. J. *J. Am. Chem. Soc.* **1984**, *106*, 6162.
(33) Ravey, J. C.; Stébé, M. J. *Prog. Colloid Polym. Sci.* **1987**, *73*, 127.
(34) Barret, E. P.; Joyner, L. G.; Halenda, P. P. *J. Am. Chem. Soc.* **1951**, *73*, 37.
(35) Alibrahim, M.; Stébé, M. J.; Dupont, G.; Ravey, J. C. *J. Chim. Phys.* **1997**, *94*, 1614.
(36) Ravey, J. C.; Stébé, M. J. In *Surfactant in Solution*; Mittal, K. L., Bothorel, P., Eds.; Plenum: New York, 1989; Vol. 79, p 272.
(37) Ropers, M. H.; Stébé, M. J. *Langmuir* **2002**, *19*, 3137.
(38) Kunieda, H.; Ozawa, K.; Huang, K. L. *J. Phys. Chem. B* **1998**, *102*, 831.
(39) Tardieu, A.; Luzzati, V. *Biochim. Biophys. Acta* **1970**, *11*, 219.
(40) Luzzati, V.; Spegt, P. *Nature (London)* **1967**, *215*, 701.
(41) Gulik, A.; Delacroix, H.; Kirschner, G. And Luzzati, V. *J. Phys. II* **1995**, *5*, 445.
(42) Sakya, P.; Seddon, J. M.; Templer, R. H.; Mirkin, R. J.; Tiddy, G. J. T. *Langmuir* **1997**, *13*, 3706.
(43) Fontell, K. *Colloid Polym. Sci.*. **1990**, *268*, 264.
(44) Chen, C. Y.; Xiao, S. O.; Davis, M. E. *Microporous Mater.* **1995**, *4*, 20.
(45) Brunauer, S.; Deming, L. S.; Deming, W. S.; Teller, E. *J. Am. Chem. Soc.* **1940**, *62*, 1723.
(46) Boissière, C.; Marines, M. A. U.; Tokumoto, M.; Larbot, A.; Prouzet, E. *Chem. Mater.* **2003.** *15*, 509.
(47) Firouzi, A.; Kumar, D.; Bull, L. M.; Besier, T.; Sieger, P.; Huo, Q.; Walker, S. A.; Zasadzinski, J. A.; Glinka, C.; Stucky, G. D. *Science* **1995**, *267*, 1138.
(48) Lee, Y. S.; Sujardi, D.; Rathman, J. F. *Langmuir* **1996**, *12*, 6202.